Structure-function analysis of the NB-ARC domain of plant disease resistance proteins

Journal of Experimental Botany, Vol. 59, No. 6, pp. 1383–1397, 2008
doi:10.1093/jxb/ern045 Advance Access publication 4 April, 2008
This paper is available online free of all access charges (see http://jxb.oxfordjournals.org/open_access.html for further details)

Journal of Experimental Botany
www.jxb.oxfordjournals.org

RESEARCH PAPER

Structure–function analysis of the NB-ARC domain of plant disease resistance proteins

Gerben van Ooijen[1,*], Gabriele Mayr[2,*], Mobien M. A. Kasiem[1], Mario Albrecht[2], Ben J. C. Cornelissen[1] and Frank L. W. Takken[1,†]

[1] *Plant Pathology, Swammerdam Institute for Life Sciences, University of Amsterdam, PO Box 94062, 1090 GB Amsterdam, The Netherlands*

[2] *Max Planck Institute for Informatics, Stuhlsatzenhausweg 85, D-66123 Saarbrücken, Germany*

Received 17 December 2007; Revised 23 January 2008; Accepted 28 January 2008

Abstract

Resistance (R) proteins in plants are involved in pathogen recognition and subsequent activation of innate immune responses. Most resistance proteins contain a central nucleotide-binding domain. This so-called NB-ARC domain consists of three subdomains: NB, ARC1, and ARC2. The NB-ARC domain is a functional ATPase domain, and its nucleotide-binding state is proposed to regulate activity of the R protein. A highly conserved methionine–histidine–aspartate (MHD) motif is present at the carboxy-terminus of ARC2. An extensive mutational analysis of the MHD motif in the R proteins I-2 and Mi-1 is reported. Several novel autoactivating mutations of the MHD invariant histidine and conserved aspartate were identified. The combination of MHD mutants with autoactivating hydrolysis mutants in the NB subdomain showed that the autoactivation phenotypes are not additive. This finding indicates an important regulatory role for the MHD motif in the control of R protein activity. To explain these observations, a three-dimensional model of the NB-ARC domain of I-2 was built, based on the APAF-1 template structure. The model was used to identify residues important for I-2 function. Substitution of the selected residues resulted in the expected distinct phenotypes. Based on the model, it is proposed that the MHD motif fulfils the same function as the sensor II motif found in AAA+ proteins (ATPases associated with diverse cellular activities)—co-ordination of the nucleotide and control of subdomain interactions. The presented 3D model provides a framework for the formulation of hypotheses on how mutations in the NB-ARC exert their effects.

Key words: Intramolecular interactions, MHD motif, NB-ARC domain, plant disease resistance, protein structure, R proteins, signal transduction, site-directed mutagenesis.

Introduction

To deal with pathogens, plants have evolved an advanced immune system to counteract pathogen attack. This immune system enables plants to discriminate between self and non-self, and to induce specific defence responses upon pathogen perception. Recognition of non-self can be mediated by so-called resistance or R proteins (Martin *et al*., 2003). Upon recognition of specific pathogen-derived molecules, called avirulence (AVR) proteins, R proteins trigger the induction of plant defences to restrict pathogen proliferation (DeYoung and Innes, 2006; Jones and Dangl, 2006). A hallmark of R protein-mediated resistance is the hypersensitive response (HR), often visible as a localized cell death response around the infection site.

Over the last decade, many *R* genes have been cloned and the majority is predicted to encode intracellular multi-domain proteins (Martin *et al*., 2003; van Ooijen *et al*., 2007). These R proteins contain a C-terminal leucine-rich

* These authors contributed equally to this work.
† To whom correspondence should be addressed. E-mail: takken@science.uva.nl

Abbreviations: AAA+, ATPases associated with diverse cellular activities; ARC, APAF-1, R proteins, and CED-4; AVR, avirulence; CC, coiled-coil; CED-4, *Caenorhabditis elegans* death-4 protein; HR, hypersensitive response; LRR, leucine-rich repeat; MHD, methionine–histidine–aspartate; MSA, multiple sequence alignment; NACHT, NAIP, CIITA, HET-E, and TP1; NB, nucleotide-binding; NOD, nucleotide-oligomerization domain; R, resistance; TIR, toll, interleukin-1, and R proteins.

repeat (LRR) domain fused to a central nucleotide-binding (NB) domain (NB-LRR proteins). The core nucleotide-binding fold in NB-LRR proteins is part of a larger entity called the NB-ARC domain because of its presence in APAF-1 (apoptotic protease-activating factor-1), R proteins and CED-4 (*Caenorhabditis elegans* death-4 protein) (van der Biezen and Jones, 1998). Structurally related domains, named NACHT (NAIP, CIITA, HET-E, and TP1) or NOD (for nucleotide-oligomerization domain), can be found in other metazoan proteins. Many of these proteins act as receptors sensing intracellular perturbations (Leipe *et al*., 2004; Ting *et al*., 2006; Rairdan and Moffett, 2007). As in R proteins, the NACHT or NOD domains in these proteins are fused to a repeat structure such as an LRR or WD40 repeat (Leipe *et al*., 2004).

No plant NB-ARC domain crystal structure has been published, but for the human NB-ARC protein APAF-1 such a structure has been solved and was found to contain a bound ADP (Riedl *et al*., 2005). This 3D structure revealed that the NB-ARC domain is actually composed of four distinct subdomains: the nucleotide-binding (NB) fold and ARC1, -2, and -3 subdomains. ARC1 forms a four-helix bundle, ARC2 adopts a winged-helix fold, and ARC3 constitutes another helical bundle. Specific ADP-binding is achieved through eight direct and four H_2O-mediated interactions with various conserved residues present in the NB, ARC1, and ARC2 subdomains (Riedl *et al*., 2005). In *C. elegans* CED-4 (Yan *et al*., 2005) and plant NB-LRR R proteins, ARC1 and ARC2 are conserved, whereas ARC3 is absent (Albrecht and Takken, 2006). Numerous conserved motifs (hhGRExE, Walker A or P-loop, Walker B, GxP, RNBS-A to D, and MHD) have been identified throughout the NB-ARC domain in R proteins (Meyers *et al*., 1999; Pan *et al*., 2000). The functional importance of these motifs is exemplified by the many mutations of motif residues that were demonstrated to result in either loss-of-function or autoactivation of the NB-LRR protein (Grant *et al*., 1995; Salmeron *et al*., 1996; Dinesh-Kumar *et al*., 2000; Tao *et al*., 2000; Axtell *et al*., 2001; Bendahmane *et al*., 2002; Tameling *et al*., 2002, 2006; Tornero *et al*., 2002; de la Fuente van Bentem *et al*., 2005; Howles *et al*., 2005; Ade *et al*., 2007; Gabriëls *et al*., 2007). Autoactivation means that HR is initiated in the absence of pathogen or AVR protein.

The identification of loss-of-function mutations in the nucleotide-binding pocket indicated that nucleotide binding is important for NB-LRR R protein function (Tameling *et al*., 2002). Previous studies have indeed confirmed that the NB-ARC domain in the R proteins I-2 and Mi-1 binds nucleotides *in vitro*. This nucleotide binding is required for I-2 function since a P-loop mutant impaired in binding is inactive (Tameling *et al*., 2002). R proteins have also been demonstrated to hydrolyse ATP *in vitro*. Two I-2 autoactivating mutants with specific point mutations in the NB subdomain were found to have wild-type nucleotide-binding affinities, but to exhibit reduced ATPase activity (Tameling *et al*., 2006).

Whereas the NB subdomain forms a catalytic nucleotide-binding and nucleotide-hydrolysing pocket, our understanding of the role of the adjacent ARC1 and ARC2 subdomains in regulation of R protein activity is limited. No autoactivating mutations have been described in the ARC1 subdomain but eight loss-of-function mutations are known (Grant *et al*., 1995; Bendahmane *et al*., 2002; Tornero *et al*., 2002). Since the ARC1 subdomain of the potato NB-LRR protein Rx has been shown to interact with various LRR domains (Rairdan and Moffett, 2006), it was proposed to have merely a structural role and to act as molecular scaffold for LRR binding.

In contrast to the ARC1, many autoactivating mutations have been identified in the ARC2 subdomain, the majority of them maps to a highly conserved carboxy-terminal motif named after its consensus sequence methionine–histidine–aspartate; the MHD motif. An aspartate to valine substitution in the MHD motif in Rx resulted in autoactivation upon transient expression in *Nicotiana benthamiana* leaves (Bendahmane *et al*., 2002). Later on, mutation of D was shown to result in autoactivation in other R proteins like I-2 and L6 (de la Fuente van Bentem *et al*., 2005; Howles *et al*., 2005) and in the NB-ARC protein NRC1 (Gabriëls *et al*., 2007). Extensive domain-swap studies using Rx and the related Gpa2 protein suggested that the ARC2 subdomain, via its interaction with the LRR, transduces pathogen recognition by the LRR domain into R protein activation (Rairdan and Moffett, 2006). ARC2 thus seems crucial to condition both autoinhibition in the absence of a pathogen, as well as activation of the R protein in the presence of a pathogen.

To gain more insight into a possible key regulatory role of ARC2 and to investigate the role of the MHD motif in more detail, additional mutations were generated in the MHD motif of the R proteins I-2 and Mi-1 and these proteins were transiently expressed in *N. benthamiana*. To link the role of the MHD motif to the nucleotide-binding properties of the NB subdomain, double mutants were made that combine the known autoactivation mutations in the NB-subdomain of I-2 to those in the MHD motif.

To elucidate further the molecular role of the MHD motif in R proteins, an *in silico* analysis was performed. The crystal structure of APAF-1 (Riedl *et al*., 2005) was chosen to model the 3D structure of the NB-ARC domain of I-2. This 3D model of the NB-ARC domain of I-2 provides a useful additional view of the functional role of the MHD motif and explains the effect of other autoactivating and loss-of-function mutants in structurally related NB-ARC proteins.

Materials and methods

Construction of vectors

Wild-type I-2 (wp42) and derived mutants D495V (wp45), S233F (wp54), and D283E (wp60) in pGreen (Hellens *et al*., 2000) have been described (Tameling *et al*., 2002, 2006; de la Fuente van Bentem *et al*., 2005). All oligonucleotides (marked FP) used in this study were purchased from MWG, Germany, and are listed in Table S1 in Supplementary data available at *JXB* online. I-2^{D495V} was combined with I-2^{S233F} or I-2^{D283E} by swapping a 0.8 kb *Sal*I/*Bam*HI fragment from wp54 and wp60 into wp45. To make the double I-2$^{S233F/D283E}$ mutant a three-point ligation was performed: wp45 was digested with *Sal*I/*Acc*65I, and fragments of wp60 (*Acc*65I/*Bst*XI) and wp54 (*Sal*I/*Bst*XI) were inserted to obtain I-2$^{S233F/D283E}$.

To generate the H494 mutant library the I-2 coding sequence was PCR amplified from wp42 using primers FP794 and FP796, and gateway *att*B flanks were introduced in a second amplification using FP872 and FP873. The resulting PCR product was recombined into pDONR207 (Invitrogen) via a Gateway BP clonase (Invitrogen) reaction to obtain pMK13.

To establish random mutagenesis of residue 494, a degenerate primer FP1158 containing NNS as a codon for residue 494 was used in combination with FP490. The 336 bp PCR product obtained was subsequently used as a mutagenic megaprimer (Ke and Madison, 1997) in combination with FP216, to amplify a 0.8 kb fragment from wp42. This fragment was digested with *Bam*HI/*Nde*I and ligated into pMK13 using the same sites, and subsequently recombined to binary vector CTAPi (Rohila *et al*., 2004) using a Gateway LR reaction (Invitrogen, Carlsbad, USA). Because the I-2 sequence contains its endogenous stop codon there is no translational fusion to the TAP tag.

pMK13 was used as a template for circular mutagenesis (Hemsley *et al*., 1989) to generate I-2 mutants W229A, V232A, W285A, R313A, and S474A using primer pairs FP1834/FP1835, FP1836/FP1837, FP1838/FP1839, FP1840/FP1841, FP1844/FP1845, respectively. The resulting mutant isoforms were subsequently recombined to CTAPi (Rohila *et al*., 2004) by a Gateway LR reaction (Invitrogen).

Creation of pSE23, a binary construct containing Mi-1, under control of its endogenous promoter, and the Mi-1^{T557S} mutation has been described before (Gabriëls *et al*., 2007). The coding sequence of Mi-1, including its stop codon and intron, was amplified from pSE23 by PCR using primers FP764 and FP766, and Gateway *att*B flanks were added by adapter PCR, using primers FP872 and FP873. The PCR product was transferred to binary vector CTAPi (Rohila *et al*., 2004) by the Gateway one-tube protocol for cloning *att*B-PCR products directly into destination vectors (Invitrogen) to create pG74.

Mi-1 D841V was generated using pG74 as a template for mutagenic overlap extension PCR (Higuchi *et al*., 1988) using primer sets FP860/FP873 and FP861/FP872. Likewise, the constructs containing Mi-1 H840R, H840V, H840stop, and H840Q were generated using overlap extension with sets of either wild-type primer FP872 or FP873 in combination with mutagenic primers FP1543/FP1544, FP1545/FP1546, FP1547/FP1548, and FP1581/FP1582, respectively. The resulting 3.8 kb products were digested with *Bsp*119I/*Eco*72I and cloned into pG74 cut with the same enzymes.

pG104 was obtained by ligating a 3.3 kb *Bam*HI/*Sal*I-digested Mi-1 PCR product that was amplified with FP1095 and FP211 into pGEX-4T-1 (GE Healthcare) digested *Bam*HI/*Xho*I. To construct Mi-1^{H840A}, pG104 was used as a template for circular mutagenesis (Hemsley *et al*., 1989). The mutation was introduced using primer set FP1100/FP1103 to create pG109. An *Eco*72I/*Bsp*119I fragment was exchanged between pG109 and pG74 to obtain Mi-1^{H840A}.

For heterologous Mi-1 protein production in *Escherichia coli* for rabbit immunization, plasmid pKG6210 (Keygene N.V.) containing genomic Mi-1 promoter and coding sequence was used to transfer an Mi-1 *Nco*I/*Bsm*I fragment into pAS2-1 (Clontech Laboratories)-digested *Nco*I/*Sma*I to obtain pSE06. An *Msc*I/*Sal*I fragment from pSE06 was ligated in pGEX-KG (Guan and Dixon, 1991) digested *Sma*I/*Sal*I to obtain pG01.

Rpi-blb1 constructs are amplified using FP771 and FP793 from pBINPLUS-RGA2-blb (van der Vossen *et al*., 2003). Gateway adapters were added to the coding sequence using FP872 and FP873, and the product was cloned into pDONR207 via a Gateway BP reaction to create pO2. Mutation D475V was introduced using the megaprimer method (Ke and Madison, 1997). The megaprimer was generated using primers FP754 and FP755 and, after purification, the fragment was extended using FP756. The product was digested with *Eco*RI/*Bgl*II, and this 1.6 kb insert is ligated in a three-point ligation with pO2 fragments generated by *Eco*RI/*Pst*I and *Pst*I/*Bgl*II to obtain pDONR207 containing Rpi-blb1^{D475V} with an intact stop codon. The insert was transferred to binary vector CTAPi in a Gateway LR reaction (Invitrogen).

Correct sequences of all clones were confirmed by sequencing.

Agrobacterium-*mediated transient transformation and protein extraction*

Agrobacterium tumefaciens strain GV3101(pMP90) (Koncz and Schell, 1986) was transformed with binary constructs (Takken *et al*., 2000) and grown to OD_{600}=0.8 in YEB medium supplemented with 20 μM acetosyringone and 10 mM MES, pH 5.6. Cells were pelleted and resuspended in infiltration medium (1× MS, 10 mM MES pH 5.6, 2% w/v sucrose) and infiltrated at OD_{600}=0.2 (for I-2, Rx, and Rpi-blb1 constructs) or 1 (for Mi-1 constructs) into 4-week-old *Nicotiana benthamiana* leaves. These ODs have been experimentally determined to result in a consistent cell death response of autoactivating mutant alleles.

For protein extraction, nine independent leaves were harvested and pooled 24 h after agroinfiltration and frozen in liquid nitrogen. After grinding the tissue, it was allowed to thaw in 2 ml protein extraction buffer per gram of tissue (25 mM TRIS pH 7.5, 1 mM EDTA, 150 mM NaCl, 10% glycerol, 5 mM DTT, 1× Roche complete protease inhibitor cocktail, and 2% PVPP). Extracts were cleared by centrifugation at 12 000 *g* at 4 °C for 10 min and the supernatant was passed over four layers of Miracloth to obtain a total protein lysate. Samples were mixed with Laemmli sample buffer, and equal amounts of total protein were run at 8% SDS–PAGE gels and blotted on PVDF membranes using semi-dry blotting. Equal loading was assayed by Ponceau S staining of Rubisco. The blocking agent used was 5% skimmed milk powder.

Trypan blue staining

Leaves were boiled for 5 min in a 1:1 mixture of ethanol and 0.33 mg ml^{-1} trypan blue in lactophenol, and destained overnight in 2.5 g ml^{-1} chloral hydrate in dH_2O.

Multiple sequence alignment of the MHD motif

R-protein sequences found in the NCBI database (accession numbers of all proteins are listed in Table S2 in Supplementary data available at *JXB* online) were aligned using the MacVector ClustalW analysis tool (Oxford Molecular Group). The aligned sequences are sorted according to a phylogenetic tree constructed by Neighbor–Joining and midpoint-rooting in MacVector.

Antibody production

Anti-I-2 was produced in rabbit by Eurogentec, Seraing, Belgium, against synthetic peptide FEKVPNPSKRNIEE, which maps just the N-terminal of the MHD motif and was affinity purified.

pG01 was transformed to *E. coli* BL21 (DE3) and expression of fusion protein GST-Mi-1, amino acids 161–899, was induced by addition of IPTG. The fusion protein was isolated using glutathione sepharose (GE Healthcare). The Mi-1 part was released from the glutathione beads using biotinylated human thrombin (Sigma). Thrombin was subsequently removed using streptavidin beads (Stratagene). Immunization was performed by injecting twice 250 μg purified Mi-1 (amino acids 161–899) protein into two New Zealand White rabbits with a 12 week interval. Fourteen weeks after the first injection, serum was collected and analysed for specific cross-reactivity to purified Mi-1 in comparison to the pre-immune sera. Serum showing the highest signal was used to detect Mi-1 *in planta*. For western blot detection, both the Mi-1 antibody and the secondary antibody goat anti-rabbit (Rockland Inc.) were used in a dilution of 1:4000 in PBST.

Structure-based multiple sequence alignment of the NB-ARC domain

A multiple sequence alignment of the following R proteins and related sequences were created from the UniProtKB database using the program MUSCLE (Edgar, 2004): human APAF-1 (O14727), tomato I-2 (Q9XET3) and Mi-1 (O81137), potato Rx (Q9XGF5), wild potato Rpi-blb (Q7XBQ9), mouse-ear cress RPM1 (Q39214), RPS2 (Q42484), and RPS4 (Q9XGM3), TMV resistance protein N (Q40392), linseed L6 (Q40253), tomato NRC1 (A1X877), *N. benthamiana* NRG1 (Q4TVR0), and nematode CED-4 (P30429). The secondary structure assignment of the PDB structure of APAF-1 (identifier 1z6t, chain A) was obtained from the DSSP database (http://www.cmbi.kun.nl/gv/dssp/) and added to the alignment. To predict the secondary structure of R proteins, the protein structure prediction server PSIPRED (http://bioinf.cs.ucl.ac.uk/psipred/) was contacted. The alignment was improved manually by minor adjustments based on structure prediction results and pairwise superposition of the PDB structures of APAF-1 (identifier 1z6t, chain A) and CED-4 (identifier 2a5y, chain B). Since the relative spatial orientation of the otherwise well-conserved NB, ARC1, and ARC2 subdomains of APAF-1 and CED-4 differs, the FATCAT program for structure superposition (Ye and Godzik, 2003), which considers conformational flexibility was applied. Subdomain borders were taken from Albrecht and Takken (2006). Shading of >60% physicochemically conserved residues was produced by GeneDoc (http://www.psc.edu/biomed/genedoc/).

3D structure model of I-2

Based on the structure-based multiple sequence alignment of the NB-ARC domain, a pairwise sequence–structure alignment of tomato R protein I-2 and human APAF-1 was constructed and formed the input into the 3D-modelling server WHAT IF (Vriend, 1990). This server returned a full-atom structure model of the NB-ARC domain of I-2. The structure of APAF-1 (PDB code 1z6t, chain A) comprises the residues 108–450 (UniProt sequence O14727) and is mapped on the I-2 residues 153–506 (UniProt sequence Q9XET3). Interatomic contacts (van der Waals interactions, salt bridges, hydrogen bonds) were calculated by the WHAT IF server (Vriend, 1990).

The protein structure image of the model was illustrated using PyMOL (http://www.pymol.org).

Results

Autoactivating aspartate-to-valine mutations in the MHD motif of Mi-1 and Rpi-blb1

Mutation of D to V in the MHD motif of the NB-LRR proteins conferring viral (Rx) or fungal resistance (I-2 and L6), and in NRC1, which is required for many R proteins to initiate HR signalling, has been shown to result in autoactivation of these proteins (Bendahmane *et al*., 2002; de la Fuente van Bentem *et al*., 2005; Howles *et al*., 2005; Gabriëls *et al*., 2007). To examine whether the D-to-V mutation also results in autoactivation in a nematode, aphid, and whitefly resistance protein (Mi-1) and an oomycete resistance protein (Rpi-blb1), the corresponding mutation was introduced in these two proteins. Autoactivation of the mutant proteins was assessed by transient *Agrobacterium tumefaciens*-mediated transformation in 5-week-old *Nicotiana benthamiana* leaves. Expression of the proteins was driven by the 35S promoter. Pictures were taken at 2 d and 4 d after agroinfiltration. Figure 1 shows that indeed Mi-1^{D841V} and Rpi-blb1^{D475V} induce an HR visible as clear necrosis of the infiltrated sector. The autoactive alleles I-2^{D495V} and Rx^{D460V} are shown as positive controls for HR development. Rx^{D460V} and Rpi-blb1^{D475V} show a rapid HR that is fully developed at 2 d (Fig. 1A), whereas Mi-1^{D841V} and I-2^{D495V} trigger a slower response that does not lead to a full necrotic sector until 3 d and 4 d after agroinfiltration, respectively (Fig. 1B). Expression of the wild-type protein does not induce HR at the indicated time points (Figs 2, 4B, and data not shown).

The observed autoactivation phenotype of the aspartate-to-valine mutants confirms an important and conserved function for D in the MHD motif of various R proteins conferring resistance to a virus (Rx), a fungus (I-2), an oomycete (Rpi-blb1), and animals (Mi-1). Apparently, mutation of this residue consistently releases R protein autoinhibition, resulting in an autoactivation phenotype or, alternatively, induces another change mimicking the activated state.

Combining autoactivating mutations in the MHD motif and the NB subdomain does not lead to an additive effect

It has been shown previously that the autoactivation phenotype of the I-2^{D495V} mutant depends on a functional

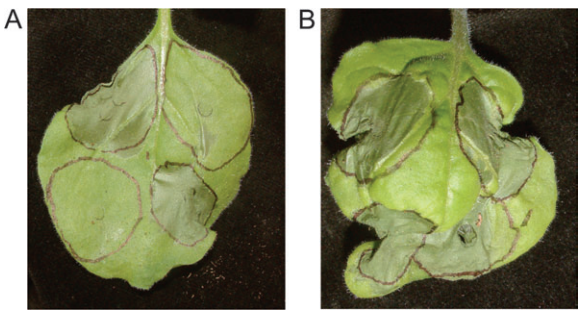

Fig. 1. Mutation of the MHD motif aspartate to valine leads to autoactivation. *Nicotiana benthamiana* leaves were agroinfiltrated with constructs to express R proteins mutated in the MHD motif (aspartate to valine). Pictures of representative leaves were taken 2 d (A) or 4 d (B) after agroinfiltration. (A) Counter-clockwise, starting from top-left: Rx^{D460V}, I-2^{D495V}, Rpi-blb1^{D475V}, Mi-1^{D841V}. (B) Counter-clockwise, starting from top-left: Mi-1^{D841V}, Rx^{D460V}, I-2^{D495V}, Rpi-blb1^{D475V}.

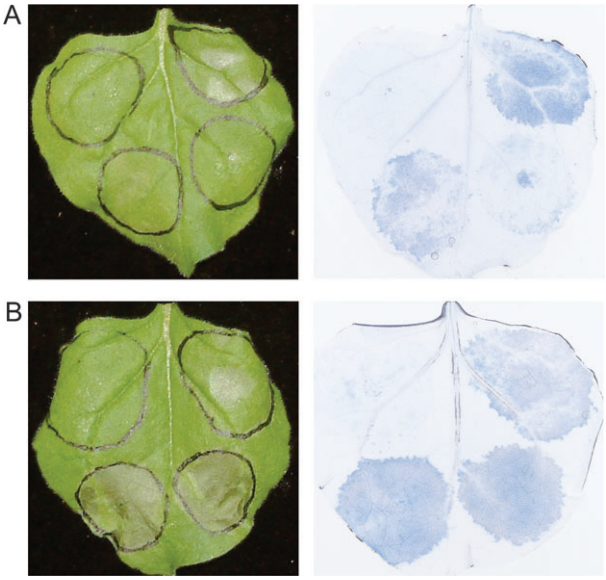

Fig. 2. Combination of autoactivation mutations in the NB and ARC2 subdomains. *Nicotiana benthamiana* leaves were agroinfiltrated with constructs to express (mutant) I-2 alleles. Representative leaves were photographed at 4 d after agroinfiltration. (A) Counter-clockwise, starting from top left: wild-type I-2, I-2^{S233F}, I-2^{D283E}, I-2$^{S233F/D283E}$. Cell death is visualized by trypan blue staining of the same leaf (right panel). (B) Counter-clockwise, starting from top left: wild-type I-2, I-2^{D495V}, I-2$^{S233F/D495V}$, I-2$^{D283E/D495V}$. Cell death is visualized by trypan blue staining of the same leaf (right panel).

nucleotide-binding subdomain since a mutant combining the D495V with the K207R mutation in the P-loop (Walker A) is inactive (Tameling *et al*., 2006). The K207R mutation in the P-loop of the NB subdomain is a loss-of-function mutation that results in strongly reduced nucleotide-binding capacity (Tameling *et al*., 2006). Two weak autoactivating mutations in I-2, D283E (in Walker B), and S233F (in RNBS-A), caused reduced ATP hydrolysis rates (Tameling *et al*., 2006). Combination of these two mutations into a double mutant is therefore predicted to result in an even more pronounced autoactivation phenotype.

To analyse whether this is the case, the mutations were combined, and timing and severity of the HR response after agroinfiltration was scored as a measure for the relative autoactivity of the I-2 mutants. As depicted in Fig. 2A, combination of both weak autoactivating NB mutations results in an additive effect. Onset of HR induced by the I-2$^{S233F/D283E}$ double mutant was consistently visible at 4 d after agroinfiltration, in five duplicate experiments each with ~10 leaves. I-2^{S233F} or I-2^{D283E} single mutants did not show HR at this time point (Fig. 2A). A trypan-blue staining of the infiltrated leaf confirms that a weak HR (cell death is visible as blue staining) is induced by the two single mutants 4 d after infiltration, whereas the HR triggered by the double mutant is much more pronounced. The wild-type I-2 protein does not induce cell death at this time-point as shown by the absence of any blue coloration. Although the I-2$^{S233F/D283E}$ double mutant is able to induce a clear HR phenotype after 4 d, the HR was never as strong as that observed for I-2^{D495V} (Fig. 1).

With the NB subdomain being the nucleotide-binding and hydrolysing site, domain swaps of Rx suggest that the ARC2 subdomain containing the MHD motif is a main regulatory element controlling R-protein activity (Rairdan and Moffett, 2006). Mutating the ARC2 MHD motif might release its negative regulatory effect on the NB, promoting the NB-ARC domain to adopt its activated conformation. To test whether the MHD mutations are dominant over the hydrolysis mutations in the NB subdomain, both autoactivating mutations were combined in I-2; the autoactivating mutation D495V in the ARC2 subdomain was paired with either the D283E or S233F in the NB subdomain. As shown in Fig. 2B, I-2^{D495V} but not wild-type I-2 induces clear necrosis 4 d after agroinfiltration. Infiltration of double mutants I-2$^{S233F/D495V}$ and I-2$^{D283E/D495V}$ consistently does not lead to an enhanced induction of HR, as confirmed by trypan-blue staining of the same leaf (Fig. 2B). Actually, the presence of a second mutation in the NB subdomain might even negatively affect R-protein activity, since the double mutants induce a lower level of cell death than the single mutant D495V does. Thus, combining the two weak autoactivating mutants with the strong autoactivating D495V mutation in ARC2 does not result in a faster or stronger HR. These data suggest that an MHD mutant reaches its maximal activation potential, and that the MHD motif is a major negative regulatory element controlling R protein activity.

Alignment of MHD motifs

Since the D-V mutation of the MHD motif has been found to result in autoactivation of all NB-LRR proteins tested so far, an extensive multiple sequence alignment (MSA) was made of the extended MHD motif of the 50 cloned NB-LRR proteins with confirmed resistance activity. The MSA is an update of a previously published MSA of this region (Howles *et al*., 2005) and includes for completeness the plant NB-LRR proteins NRC1 and NRG1 that are both involved in R protein-signalling pathways (Peart *et al*., 2005; Gabriëls *et al*., 2006). APAF-1 was included to illustrate the conservation of this motif in a sequence-related human protein. The MSA was sorted to match a phylogenetic tree that was generated based on the aligned motifs. Although phylogeny based on such a short sequence is error prone, clear clusters stand out (Fig. 3). This clustering complies with the relationships of R proteins based on the identity of their N-terminal domains. This N-terminal domain often has homology with the *Drosophila* Toll and human interleukin-1 receptors (TIR), the TIR-NB-LRRs or TNLs. As the N-terminus of the

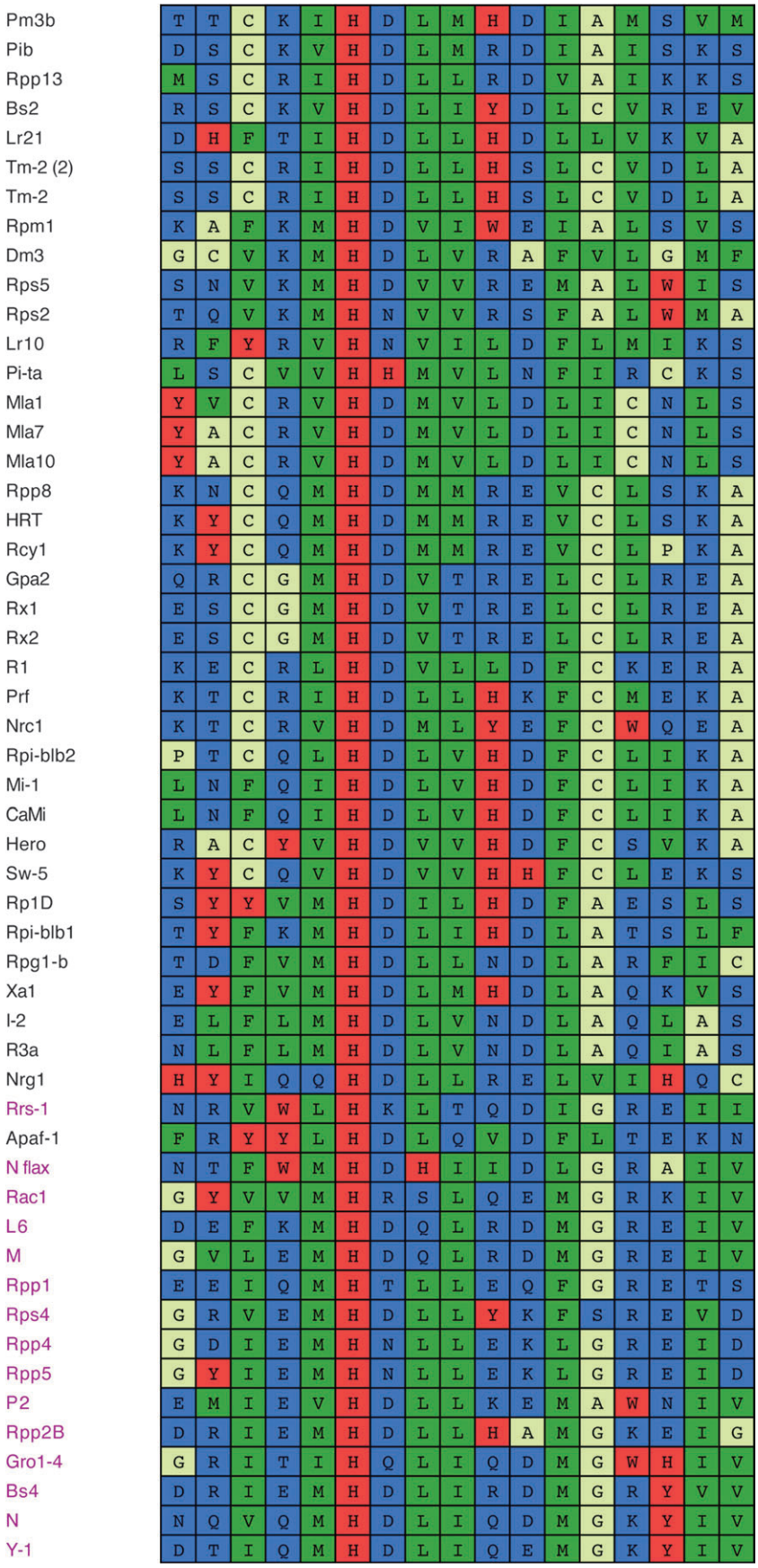

heterogeneous non-TNL group often contains predicted coiled-coil (CC) motifs, this group is referred to as CNLs (reviewed in Martin *et al*., 2003; van Ooijen *et al*., 2007). As can be appreciated from Fig. 3, the TNL group (aubergine characters) clusters and the consensus sequence of its MHD motif extends towards the carboxy-terminal end compared with those of CNLs. The conservation of this motif in human APAF-1 is clear as well.

As can be deduced from the MSA in Fig. 3, the most conserved residue in the MHD motif is the histidine that is invariable in all NB-LRR R proteins. The histidine is always N-terminally flanked by a hydrophobic residue (a methionine in 53% of the cases), whereas the C-terminal neighbouring residue is an aspartate in most cases (83%). So, although conservation of the aspartate is considerable, it is not invariant. The histidine is the only invariable residue in the MHD motif, which suggests an essential role for this residue.

Mutation of the histidine in the MHD motif

Because the histidine is the most conserved residue in the MHD motif of plant NB-LRR R proteins, it was decided to analyse the effect of mutating this residue on I-2 function. First, a small library of I-2 clones that encode proteins that are variable for residue H494 was generated. This library was made by site-directed mutagenesis using the megaprimer method (Ke and Madison, 1997). In the mutagenic primer, the H494-encoding codon (CAT) was replaced with NNS (in which N can be any nucleotide and S can be either G or C). Introduction of S reduces the number of possible codons to 32, thereby increasing the relative percentage of the single-codon amino acids tryptophan and methionine. To have a good representation of all possible codons, a ~6-fold excess of the 32 possible codons (184 clones) was sequenced. The variants obtained, and the number of clones coding for each amino acid at position 494, are shown in Table 1. Of the 19 possible amino acid replacements plus three stop codons, isoleucine was the only one that was not present in the sequenced set of clones. An over-representation of the wild-type histidine residue was obtained, probably due to inefficient removal of the wild-type insert.

The phenotype of the H494 variants was analysed by transient expression in *N. benthamiana* leaves using agroinfiltration and assessment of timing and extent of cell death of the infiltrated region. Except for stop codon mutants and the wild type, HR was not observed when a glutamate, leucine, or tryptophan replaced the histidine at position 494. The 15 other replacements resulted in autoactivation. However, variation in the amplitude of timing and intensity of HR was observed (Table 1). The results in Table 1 represent the average observed effects of at least two independent clones where possible. HR was ranked from very strong (+++) to no visual effect (–). To illustrate the range of HR, Fig. 4A shows I-2 mutants H494A (+++), H494R (++), H494V (+), H494F (+/–), H494L (–), and H494Q (–). The same activity range is also evident upon trypan blue staining of this leaf (Fig. 4A, right panel). Substitution of H494 for alanine reproducibly resulted in the fastest induction of HR. Limited cell death was also visualized upon expression of I-2^{H494L} and I-2^{H494Q}. However, since the intensity of the blue staining was comparable to that for wild-type I-2, it probably represents background staining. The cell death staining intensity of infiltrated regions depicted in this figure cannot be directly compared with those in Figs 1 and 2, since a different expression vector was used in these experiments.

To investigate whether corresponding mutations in a related NB-LRR protein, Mi-1, confer similar phenotypes as obtained for I-2, Mi-1 MHD motif mutants H840A, H840R, H840V, H840Q, and, as a negative control, H840stop were generated. Similar to I-2, Mi-1^{H840A} leads to the strongest autoactivation (Fig. 4B), whereas Mi-1^{H840R} and Mi-1^{H840V} show intermediate phenotypes. Wild-type Mi-1 and Mi-1^{H840Q} do not induce HR, but induce a similar light-blue staining as the Mi-1^{H840stop} control.

Autoactivation by Mi-1 MHD mutants is not due to higher expression levels in the plant

To test whether autoactivation induced by mutations in the MHD are due to differences in protein expression levels rather than a direct effect of the mutation, the expression levels of the various mutants were analysed. To detect the R proteins after *in planta* expression, antibodies against I-2 and Mi-1 were raised in rabbit. Either a synthetic I-2 peptide or the Mi-1 NB-ARC domain with part of its N-terminal flanking sequence (Mi-1 amino acids 161–899) was used as antigen. The latter recombinant Mi-1 protein was heterologously produced in *E. coli* as described in the Materials and methods. Using affinity-purified I-2 antibodies, it was not possible to detect the R protein in protein extracts isolated from agroinfiltrated *N. benthamiana* leaves, although the antibody successfully recognized *E. coli*-produced I-2 protein

Fig. 3. Multiple sequence alignment of the MHD motif. Multiple sequence alignment of the extended MHD motif in 50 R proteins with confirmed resistance activity, the downstream resistance signalling NB-ARC-LRR proteins NRC1 and NRG1, and human APAF-1. CC-NB-LRR proteins are marked in blue and TIR-NB-LRR proteins in red. Amino acid residues are coloured based on their chemical type: cream, small hydrophobic (A, C, G, P); blue, hydrophilic (D, E, K, N, Q, R, S, T); red, aromatic (H, W, Y); green, large hydrophobic (F, I, L, M, V). Names of TNLs are in aubergine lettering, CNLs in black.

Table 1. *Substitutions of I-2 H494*

Amino acid		No. of clones	Phenotype
A	Alanine	5	+++
C	Cysteine	1	++
D	Aspartic acid	8	++
E	Glutamic acid	2	++
G	Glycine	10	++
K	Lysine	3	++
N	Asparagine	1	++
R	Arginine	13	++
S	Serine	7	++
T	Threonine	7	++
V	Valine	6	++
M	Methionine	2	+
Y	Tyrosine	4	+
F	Phenylalanine	4	+/–
P	Proline	3	+/–
L	Leucine	12	–
Q	Glutamine	5	–
W	Tryptophan	1	–
I	Isoleucine	0	nd
H	Histidine	85	–
*	Stop	5	–

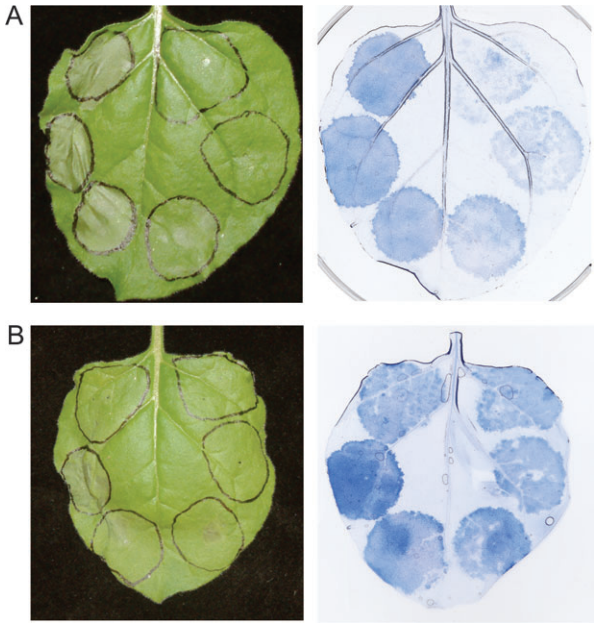

Fig. 4. Mutation of the MHD motif histidine leads to a range of autoactivating phenotypes. *Nicotiana benthamiana* leaves were agroinfiltrated with constructs to express I-2 or Mi-1 mutants variant for the MHD motif histidine. (A) I-2 mutants variant for H494. Counter-clockwise, starting from top left: I-2^{H494A}, I-2^{H494R}, I-2^{H494V}, I-2^{H494F}, I-2^{H494L}, I-2^{H494Q}. The picture was taken 4 d after agroinfiltration. Cell death is visualized by trypan blue staining of the same leaf (right panel). (B) Mi-1 mutants variant for H840. Counter-clockwise, starting from top left: wild-type Mi-1, Mi-1^{H840A}, Mi-1^{H840R}, Mi-1^{H840V}, Mi-1^{H840Q}, Mi-1^{H840stop}. The picture was taken 4 d after agroinfiltration. Cell death is visualized by trypan blue staining of the same leaf (right panel).

(data not shown). It is likely that I-2 expression levels *in planta* are below the detection level of the I-2 antibody (data not shown; Tameling *et al*., 2006). Efforts to detect N- or C-terminally epitope-tagged I-2 failed and, since all tags tested rendered the autoactivation mutant I-2^{D495V} inactive, these efforts were not continued.

In contrast to I-2, *in planta* produced Mi-1 could readily be detected using the Mi-1 antibody. The Mi-1 antibody detects both full-length Mi-1 and a truncated version lacking the LRR in total protein extracts from *N. benthamiana* leaves, following transient expression using agroinfiltration (Fig. S1 in Supplementary data available at *JXB* online). No Mi-1-specific bands were detected on western blots from protein extracts of leaves agroinfiltrated with Mi-1 LRR (amino acids 900–1257), showing specificity of the antibody for the N-terminal part of Mi-1. Besides the Mi-1 protein, a ~80 kDa band was consistently found in all *N. benthamiana* extracts, including these from non-infiltrated leaves. The nature of this *N. benthamiana*-specific protein is not known, but like Mi-1 it was not recognized on blots incubated with pre-immune serum (Fig. S1).

To analyse the expression levels of Mi-1 mutants, constructs encoding Mi-1^{D841V} and H840 mutants showing strong (H840A), intermediate (H840V), or no (H840Q) autoactivating phenotype were agroinfiltrated. Infiltrated leaves were harvested after 24 h, well before onset of HR, and subsequently used for total protein extraction. For comparison, the expression level of wild-type Mi-1 was included. To confirm equal loading, a western blot of total soluble protein from agroinfiltrated leaves was stained with Ponceau S. This blot was subsequently probed with the Mi-1 antibody and Fig. 5 shows the Mi-1 variants migrating at the predicted weight of ~145 kDa. The expression levels of autoactivating mutants do not differ significantly from the wild-type control. These results substantiate that induction of HR by Mi-1 mutants is not caused by differences in protein level and can solely be attributed to the specific point mutations.

Structure-based multiple sequence alignment of R proteins

To provide an explanation for the phenotypes of the MHD mutants, a 3D model of the I-2 NB-ARC domain was built. To construct the structure model, sequence conservation and domain organization of R proteins were examined by generating a structure-based multiple sequence alignment (Fig. 6). Two homologous proteins with known structure, human APAF-1 and *C. elegans* CED-4, were included (Riedl *et al*., 2005; Yan *et al*., 2005). The initial alignment was refined manually, taking into account secondary structure predictions of R proteins, and known structure assignments of APAF-1 and CED-4. Sequence identity between I-2 and APAF-1 NB-ARC domains is low (24%) and concentrated within or adjacent to conserved motifs present in the three subdomains of the NB-ARC domain of R proteins (Fig. 6).

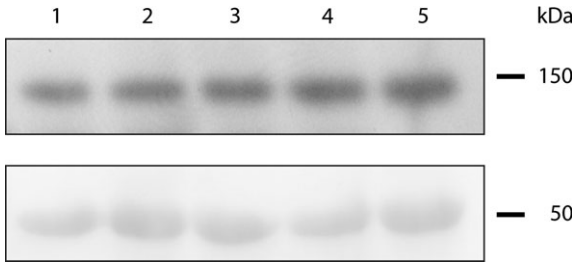

Fig. 5. Expression levels of wild-type and mutant Mi-1. *Nicotiana benthamiana* leaves were agroinfiltrated with constructs to express (mutant) Mi-1. One day after agroinfiltration, protein extracts were subjected to SDS–PAGE followed by Ponceau S staining of Rubisco (B) and immunoblotting with anti-Mi (A): 1, Mi-1 wild-type; 2, Mi-1^{D841V}; 3, Mi-1^{H840A}; 4, Mi-1^{H840V}; 5, Mi-1^{H840Q}.

It can be seen in Fig. 6 that most known R protein motifs are also conserved in APAF-1 and CED-4. The most important exception is the MHD motif itself, which is conserved in APAF-1 but not in CED-4. The RNBS-C motif is not conserved either in CED-4 and has very low conservation in APAF-1. Only two residues of this motif are in common with R proteins. The RNBS-D is conserved neither in CED-4 nor in APAF-1. In the APAF-1 crystal structure, the corresponding region is not involved in formation of the ADP-binding pocket and is located on a helix within ARC2. Another remarkable difference between APAF-1/CED-4 and R proteins is a loop connecting the ARC1 and ARC2 subdomains (thin yellow line in Fig. 6), which is considerably shorter in R proteins. Despite these differences, a remarkable conservation of the residues forming the nucleotide-binding pocket is observed. This is illustrated in Fig. 6, where all residues are marked that are conserved in R proteins. Most of these amino acids are located in previously defined motifs, except for APAF-1 serine 422 in the ARC2 subdomain. This serine participates in a water-mediated hydrogen bond to the ADP ribose. A direct hydrogen bond with the β-phosphate of ADP was observed for histidine 438 in the APAF-1 MHD motif (Riedl *et al*., 2005). These two important amino acids as well as most of the other conserved ADP-binding pocket residues are missing in CED-4. The ARC2 subdomain in R proteins is generally more similar to APAF-1 than to CED-4. In conclusion, the conserved cluster of residues in the ADP binding pocket make the APAF-1 ADP-bound structure the preferable modelling template for the NB-ARC domain of R proteins.

Protein structure model of I-2 and localization of mutations

Based on the multiple sequence alignment (Fig. 6), a similar secondary structure and a conserved 3D arrangement of protein subdomains and nucleotide-binding mode in the NB-ARC domain of R proteins as found for ADP-bound APAF-1 is proposed. Therefore, this APAF-1 crystal structure (PDB code 1z6t, chain A) was chosen as modelling template for I-2 (Fig. 7; see Fig. S2 in Supplementary data at *JXB* online). As in the case of the APAF-1 NB-ARC domain, in the NB-ARC structural model of I-2 the ADP molecule is deeply buried in a pocket formed at the interface of the NB, ARC1, and ARC2 subdomains.

Mapping of known loss-of-function mutations identified in the NB-ARC domains of R proteins reveals that they are located at many different positions scattered throughout the molecule (Fig. 6, motifs indicated in Fig. 7; Takken *et al*., 2006). When located in the ADP-binding pocket, the loss-of-function mutations point to the adenosine binding site of the pocket, possibly affecting ADP binding. This observation agrees well with the finding that nucleotide binding is essential for R protein function (Tameling *et al*., 2006).

In contrast to loss-of-function mutations, autoactivating mutations are exclusively located on the opposite side of the interface between the NB and ARC2 subdomains. Here, they map in, or close to, the ADP-binding pocket where they are located near the phosphates, which suggests a role in phosphate binding and/or hydrolysis (Fig. 7). This is in good agreement with the observation that hydrolysis mutants are autoactivating (Tameling *et al*., 2006).

Specific point mutations substantiate the I-2 NB-ARC structure model

The observed clustering of autoactivating mutations suggests that the model depicted in Fig. 7 is a reliable representation of the NB-ARC domain of R proteins. To test this reliability, residues were selected that are predicted to be important for R protein activity based on their high conservation in the alignment and their prominent structural position in the 3D model. Five mutations were selected at predicted important structural positions (see Fig. S2 in Supplementary data at *JXB* online). One mutation (R313A) was made in the sensor I motif and is a predicted loss-of-function mutant. Three mutations were made at the interface of the NB and ARC2 (i.e. W229A, V232A, and W285A) that are predicted to affect I-2 function. One mutation, S474A, maps outside this interface and is poorly conserved. Therefore, this residue is predicted to be of little functional importance and not to effect R protein function.

As shown in Fig. 8A, expression of the I-2^{R313A} sensor I mutant induces less cell death (visualized by trypan blue) than expression of wild-type I-2 from the same binary vector. This observation suggests that the mutant is affected in its ability to induce cell death and might represent a loss-of-function mutant. Of the other three mutants with predicted functional relevance, I-2^{V232A} was

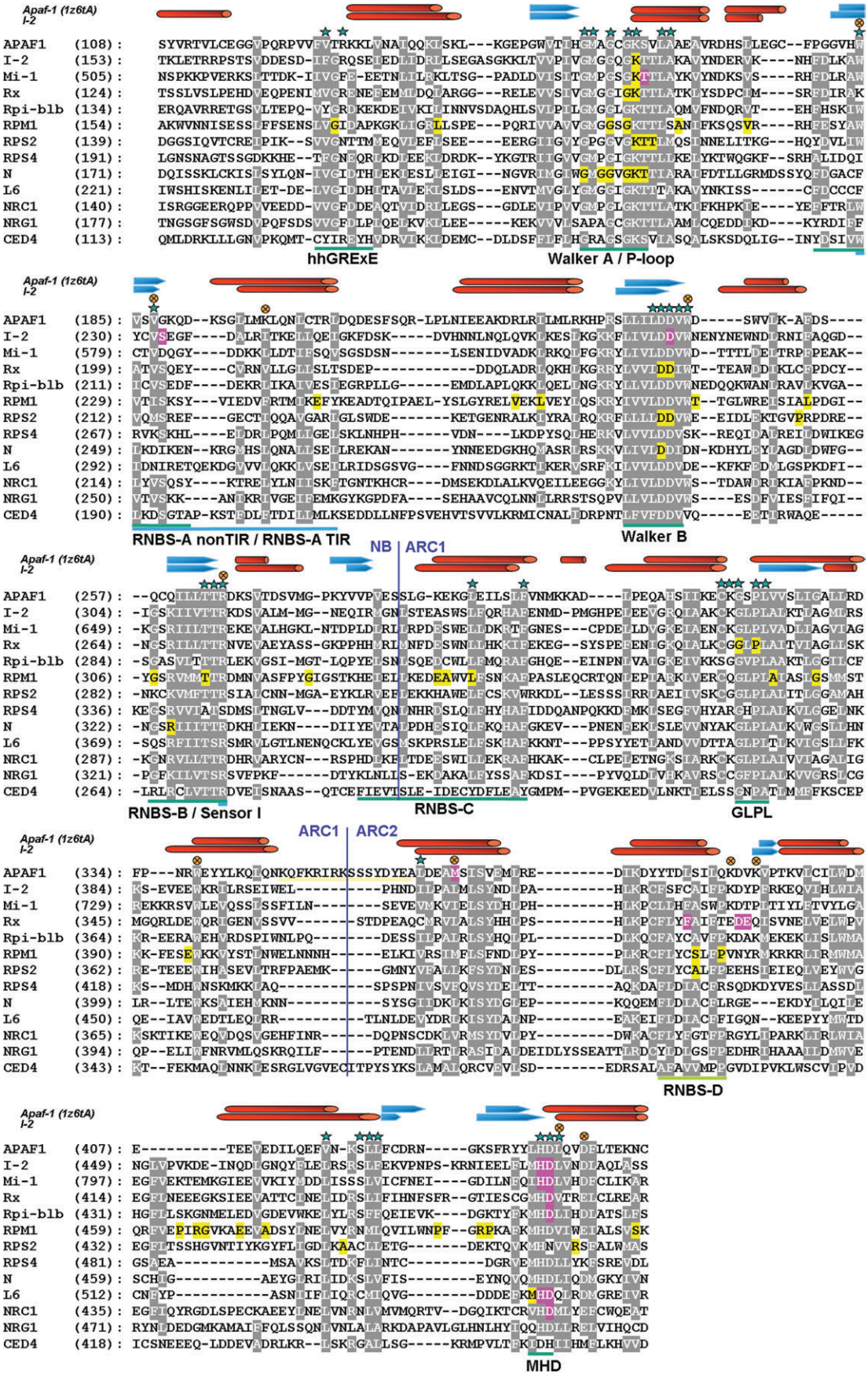

found to represent an autoactivation mutant triggering clear HR (Fig. 8B), whereas W229A and W285A probably represent loss-of-function mutants (Fig. 8C, D). As expected, the I-2^{S474A} mutant is indeed neither gain- nor loss-of-function as it behaves in a similar way to the wild-type I-2 protein (Fig. 8E). Note that mild autoactivity, inducing limited cell death, was consistently observed upon expression of wild-type I-2 using the CTAPi binary vector (Rohila *et al*., 2004). This cell death was not triggered when wild-type I-2 was expressed using the pGreen backbone (Hellens *et al*., 2000) as used in Figs 1 and 2. Similar quantitative differences were observed with Mi-1, and are consistent with the higher expression levels observed for Mi-1 and other transgenes when expressed from the CTAPi vector (data not shown).

The mutational analysis supports the use of the NB-ARC model presented in Fig. 7 to locate residues important for R-protein function. The model can also be used to formulate hypotheses to explain R protein mutant phenotypes, as discussed below.

Discussion

The central NB-ARC domain in R proteins has been proposed to function as a molecular switch that, depending on the nucleotide bound, defines the activation state of the R protein (Rairdan and Moffett, 2006; Takken *et al*., 2006; Tameling *et al*., 2006; Ade *et al*., 2007). In this functional model, the NB subdomain is the catalytic core, the ARC1 subdomain is required as a scaffold for the intramolecular interaction with the LRR, and the ARC2 subdomain is the regulatory element that transduces pathogen perception by the LRR into R-protein activation (Rairdan and Moffett, 2006; Tameling *et al*., 2006). To examine how the ARC2 regulates R-protein activity, it was decided to focus on the MHD motif located in this subdomain. The results presented here indicate that the histidine in the MHD motif is a key component of the 'switch' of R-protein activity.

Functional roles of the MHD residues

Both the histidine and the aspartate in the MHD motif are among the most conserved residues in R proteins, pointing to an important functional and structural role (Figs 3, 7). As part of a framework of conserved amino acids in the deeply buried ADP-binding pocket, the histidine is in a critical position (Fig. 7). Its location suggests that it fulfils the same role as proposed for the corresponding histidine in APAF-1, which is to bind and position the β-phosphate of the ADP (Riedl *et al*., 2005; Albrecht and Takken, 2006). A direct interaction of the winged-helix domain with the nucleotide via a histidine is a unique feature of APAF-1 and is not found in related ATPases associated with diverse cellular activities (AAA+) (Riedl *et al*., 2005). The latter use a conserved arginine residue in the so-called sensor II motif in the helical bundle (corresponding to the ARC1 subdomain) to co-ordinate the bound nucleotide and control intersubunit interactions (Ogura *et al*., 2004). No clear sensor II motif is present in proteins like APAF-1 and R proteins, but its function might be taken over by the MHD motif. In APAF-1, the binding of H438 to the beta-phosphate of the ADP stabilizes the compact closed conformation of the NB-ARC domain (Riedl *et al*., 2005). Through ADP binding, the histidine participates in the interaction between the NB and the ARC2 subdomains. Mutation of the MHD histidine and aspartate may weaken ADP–protein and subdomain interactions resulting in the destabilization of the closed ADP-bound conformation. Consequently, nucleotide exchange could be favoured, resulting in a constitutively active conformation of the R protein. In this way, the MHD motif takes over both AAA+ protein sensor II functions—co-ordination of the bound nucleotide and control of intersubunit interactions. Such a major negative regulatory role for the MHD is in line with the observation that combining an MHD mutant with a NB hydrolysis mutant does not result in an even faster HR response (Fig. 2).

The slightly reduced cell death triggered by the double mutant, compared with that of the MHD mutant, could be caused by a reduced nucleotide-binding affinity, resulting in a less potent activation of defence signalling. Detailed biochemical studies, beyond the scope of this study, using purified full-length wild-type and mutant proteins are required to test this hypothesis.

A sensor II function for the MHD motif could also explain the autoactivating phenotype obtained upon mutation of the aspartate. This aspartate is located C-terminally of the histidine at the positively charged end of an alpha-helix, a position preferably occupied by negatively charged amino acids stabilizing the helix dipole. Mutating the aspartate or any other residue at this position (Fig. 3) might reposition the helix, thereby dislocating the preceding histidine and weakening its interaction with the ADP.

Fig. 6. Structure-based multiple sequence alignment of the NB, ARC1, and ARC2 subdomains of NB-LRR R proteins, APAF-1 and CED-4. The secondary structure assignment of the APAF-1 protein (PDB code 1z6t, chain A) and the secondary structure prediction of I-2 are depicted at the top of the alignment (beta-strands in blue, alpha-helices in red). Domain borders are indicated as vertical blue lines. Motifs are annotated as horizontal green and blue lines below the aligned sequences. Amino acid positions experimentally shown to lead to an HR response are highlighted in pink, loss-of-function mutations in yellow. Amino acids located in the ADP-binding site of APAF-1 and well conserved in R proteins are marked by green stars. Residue positions of potential interest for experiments are marked by orange crossed circles.

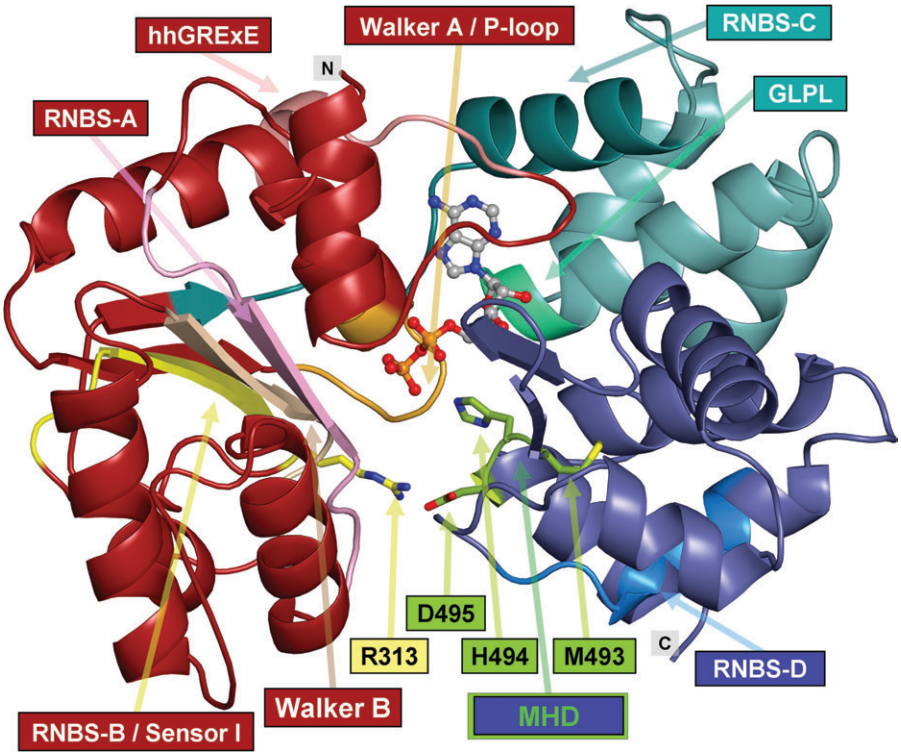

Fig. 7. Structural model of the NB-ARC domain of I-2. Computationally derived 3D structure model of the NB-ARC domain of the resistance protein I-2. The model was created using the ADP-bound structure of human APAF-1 (PDB code 1z6t, chain A) as structural template for I-2. The locations of R-protein motifs are marked with arrows. Amino acids of the MHD motif as well as the sensor I arginine are shown in stick representation. ADP atoms are depicted as balls and sticks. Subdomain colouring: NB, red; ARC1, green; ARC2, blue. Atom colouring: oxygen, red; nitrogen, blue; phosphorus, orange.

In an ADP-bound conformation, the MHD aspartate may contact the so-called sensor I arginine through a salt bridge (as predicted by the WHAT-IF server). This conserved arginine (APAF-1 R265, corresponding to R313 in I-2; Fig. 7) in the sensor I motif senses the presence of a γ-phosphate on the bound nucleotide in related AAA+ proteins and relays this information to other domains of the protein (Ogura and Wilkinson, 2001). Because only the ADP-bound structure has been solved for APAF-1, it is not known how it senses a γ-phosphate, but the corresponding arginine directly interacts with the γ-phosphate in the crystal structure of ATP-bound CED-4 (Yan *et al*., 2005). The sensor I maps to the NB subdomain and is hallmarked by the hhhhToR signature, which is referred to as the RNBS-B motif in plant R proteins (Meyers *et al*., 1998) (Fig. 6). The importance of this motif was suggested by loss-of-function mutations of the two neighbouring threonine amino acids in Rpm1 and Prf (Salmeron *et al*., 1996; Tornero *et al*., 2002) (Fig. 6), which could result in a side chain dislocation of the adjacent sensor I arginine. Direct proof for functional importance of the sensor I arginine was shown here by its substitution for an alanine. As shown in Fig. 8A, this mutation results in a loss-of-function phenotype. In light of this mutation of the MHD, aspartate might not only directly affect ADP binding through a delocalization of the preceding histidine, but could also lead by itself to a more open conformation of the NB-ARC as it can no longer interact with sensor I. An open conformation would result in weaker binding of ADP, allowing exchange for ATP and resulting in R-protein activation.

To conclude, the MHD histidine may be in direct contact with the ADP, and its mutation could directly destabilize the inactive ADP-bound protein complex, allowing nucleotide exchange and activation of the protein. Mutation of the aspartate could dislocate the histidine making it less effective in repressing the R protein and/or negatively influence the interaction between the NB and ARC2 subdomains, thereby destabilizing the closed, inactive protein conformation.

Implications of the I-2 structural model on residues outside the MHD motif

The availability of a structural model of the NB-ARC domain of R proteins allows the formation of hypotheses on the molecular mechanism underlying autoactivation phenotypes induced by mutation of residues outside the MHD motif. Most autoactivating mutations in R proteins map to the interface of the NB and the ARC2 subdomains, such as I-2^{S233F}, I-2^{D283E}, Rps5^{D266E}, Rx^{D399V}, and

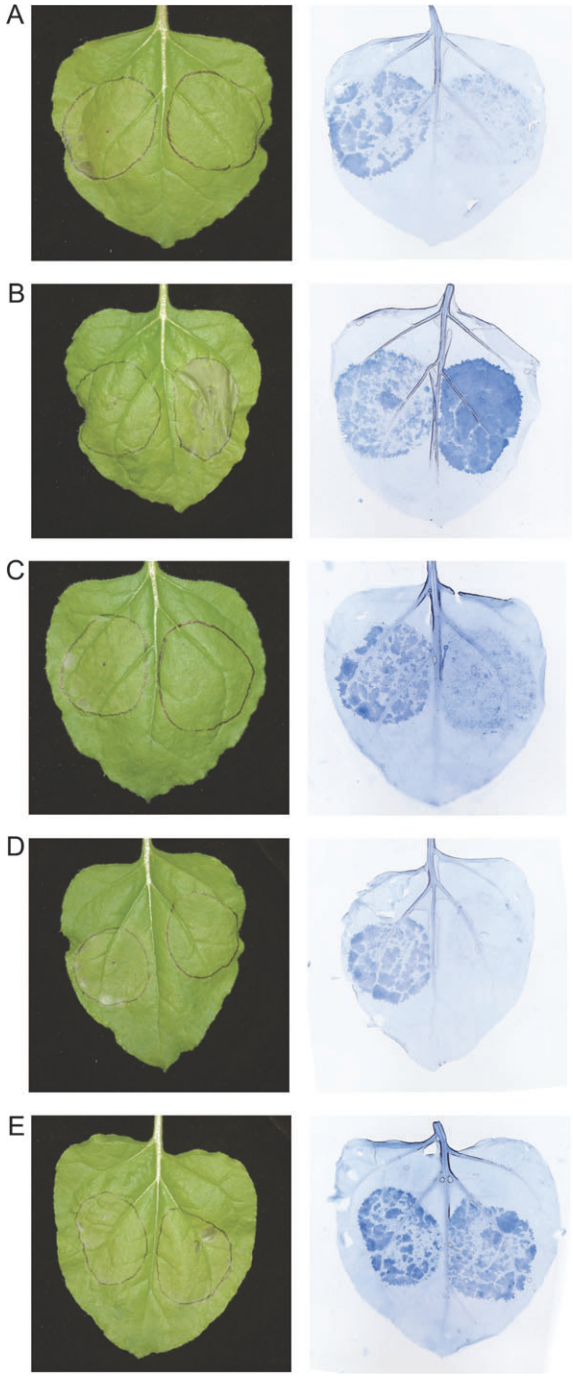

Fig. 8. Mutation of predicted important residues alters R-protein function. *Nicotiana benthamiana* leaves were agroinfiltrated with constructs to express wild-type or mutant I-2 protein. After pictures were taken 4 d after agroinfiltration (left panels), the same leaves were stained for cell death using trypan blue (right panels). Wild-type I-2 is expressed in the left leaf half, mutants in the right. (A) I-2^{R313A}, (B) I-2^{V232A}, (C) I-2^{W229A}, (D) I-2^{W285A}, (E) I-2^{S474A}.

Rx^{E400K} (Bendahmane *et al*., 2002; Tameling *et al*., 2006; Ade *et al*., 2007). The present structural model of I-2 shows that I-2 residues S233 and D283 are on the same side of the NB subdomain and are facing Rx residues D399 and E400, which are located on the opposite side, on the ARC2 subdomain.

I-2 mutations S233F and D283E in the NB subdomain (see Fig. S2 in the Supplementary data at *JXB* online) have been shown to reduce the ATP hydrolysis rate (Tameling *et al*., 2006). Rx residues D399 and E400 in Rx (Bendahmane *et al*., 2002) are relatively distant from the ATP. These residues are therefore unlikely to be directly involved in ATP hydrolysis. These ARC2 residues, however, contact the residues in the neighbouring NB subdomain and may thus be involved in stabilizing the inactive domain complex. Mutation of these residues may destabilize the inactive conformation, allowing the protein to adopt its activated state. This hypothesis is in agreement with the assumption that NB-ARC ATPases like R proteins undergo conformational changes upon activation (Moffett *et al*., 2002; Leipe *et al*., 2004; Rairdan and Moffett, 2006; Takken *et al*., 2006; Ade *et al*., 2007; Bent and Mackey, 2007; van Ooijen *et al*., 2007).

The observed spatial clustering of known autoactivating mutations in the present structural model allowed identification of additional mutations that could affect protein function (Fig. 6). These residues are amino acids that are well conserved and also in the spatial vicinity of experimentally verified sites. Their 3D locations are depicted in the structural model of I-2 (see Fig. S2 in the Supplementary data at *JXB* online). Two conserved residues were selected in the RNBS-A (W299A and V232) because of their predicted positions at the interface between NB and ARC2. Transient expression of the V232A resulted in autoactivation and an intense blue staining when stained with trypan blue (Fig. 8B). This observation supports the hypothesis that this loop is important for interactions between these two subdomains. The W229A mutant was shown to induce less cell death than wild-type I-2, suggesting that it is either hypoactive or inactive (Fig. 8C). In the NB-ARC structure (Fig. S2), this tryptophan is deeply buried and has numerous non-covalent interactions with other amino acids, for example, the Walker B D282. Mutation probably abrogates the stability of the protein fold leaving a non-functional protein.

W285 in the Walker B motif was selected because of its position near the aspartates that are required for ATPase activity. Mutation of this residue resulted in an inactive or hypoactive protein, confirming that this residue is important for function (Fig. 8D).

An intriguing difference between R proteins and APAF-1 as well as CED-4 is the loop connecting ARC1 and ARC2. In CED-4, this loop harbours a tyrosine that, together with the sensor I arginine and the P-loop lysine, is crucial for co-ordinating the gamma-phosphate of ATP (Yan *et al*., 2005). It is probable that this loop is flexible, enabling ARC2 dislocation upon activation. The loop is of

variable length, but considerably shorter in R proteins (Fig. 6; see Fig. S2 in Supplementary data at *JXB* online) and also lacks sequence conservation. In the APAF-1 structure, the loop covers part of the interface between the NB and ARC2 subdomains and is involved in interdomain reorganization upon activation. This implies that even though the proposed ADP-bound conformation of the NB-ARC domain in R proteins is similar to that of APAF-1, the ATP-bound state is likely to differ.

In conclusion, the present data support the current models for R-protein function in which the NB-ARC acts as a molecular switch (Takken *et al*., 2006; Tameling *et al*., 2006; Bent and Mackey, 2007; van Ooijen *et al*., 2007). Although a crystal structure is required to confirm the 3D model provided, it can already serve as a framework for the formulation of hypotheses on how mutations exert their effect. This structural model provides insight into the function of the conserved elements within the NB-ARC domain and sheds light on the molecular mechanisms through which R proteins orchestrate plant defence.

Supplementary data

Supplementary data can be found at *JXB* online.

Figure S1. The Mi-1 antibody specifically recognizes transiently expressed Mi-1 protein.

Figure S2. Structure model of the NB-ARC domain of I-2 indicates predicted important positions.

Table S1. Oligonucleotides used in this study.

Table S2. Accession numbers of proteins used.

Acknowledgements

We would like to thank Harold Lemereis and Ludek Tikovski for plant handling. Thijs Hendrix is acknowledged for raising the Mi-1 antibody. Martijn Rep is acknowledged for critical review of the manuscript. pKG6210 containing the *Mi-1* genomic region was provided by Keygene N.V., The Netherlands. A construct containing the *Rpi-blb1* gene was kindly provided by Dr E van der Vossen, Wageningen University, Wageningen, The Netherlands. GvO is supported by the Research Council for Earth and Life Sciences (ALW) with financial aid from the Netherlands Organization for Scientific Research (NWO). GM and MA have been financially supported by the German National Genome Research Network (NGFN). The research was conducted in the context of the BioSapiens Network of Excellence funded by the European Commission under grant number LSHG-CT-2003-503265.

References

Ade J, DeYoung BJ, Golstein C, Innes RW. 2007. Indirect activation of a plant nucleotide binding site-leucine-rich repeat protein by a bacterial protease. *Proceedings of the National Academy of Sciences, USA* **104,** 2531–2536.

Albrecht M, Takken FLW. 2006. Update on the domain architectures of NLRs and R proteins. *Biochemical and Biophysical Research Communications* **339,** 459–462.

Axtell MJ, McNellis TW, Mudgett MB, Hsu CS, Staskawicz BJ. 2001. Mutational analysis of the *Arabidopsis RPS2* disease resistance gene and the corresponding *Pseudomonas syringae avrRpt2* avirulence gene. *Molecular Plant–Microbe Interactions* **14,** 181–188.

Bendahmane A, Farnham G, Moffett P, Baulcombe DC. 2002. Constitutive gain-of-function mutants in a nucleotide binding site-leucine rich repeat protein encoded at the *Rx* locus of potato. *The Plant Journal* **32,** 195–204.

Bent A, Mackey D. 2007. Elicitors, effectors, and R genes: the new paradigm and a lifetime supply of questions. *Annual Review of Phytopathology* **45,** 399–436.

de la Fuente van Bentem S, Vossen JH, de Vries KJ, van Wees S, Tameling WIL, Dekker HL, de Koster CG, Haring MA, Takken FLW, Cornelissen BJC. 2005. Heat shock protein 90 and its co-chaperone protein phosphatase 5 interact with distinct regions of the tomato I-2 disease resistance protein. *The Plant Journal* **43,** 284–298.

DeYoung BJ, Innes RW. 2006. Plant NBS-LRR proteins in pathogen sensing and host defense. *Nature Immunology* **7,** 1243–1249.

Dinesh-Kumar SP, Tham WH, Baker BJ. 2000. Structure-function analysis of the tobacco mosaic virus resistance gene *N*. *Proceedings of the National Academy of Sciences, USA* **97,** 14789–14794.

Edgar RC. 2004. MUSCLE: multiple sequence alignment with high accuracy and high throughput. *Nucleic Acids Research* **32,** 1792–1797.

Gabriëls SHEJ, Takken FLW, Vossen JH, *et al*. 2006. cDNA-AFLP combined with functional analysis reveals novel genes involved in the hypersensitive response. *Molecular Plant–Microbe Interactions* **19,** 567–576.

Gabriëls SHEJ, Vossen JH, Ekengren SK, *et al*. 2007. An NB-LRR protein required for HR signalling mediated by both extra- and intracellular resistance proteins. *The Plant Journal* **50,** 14–28.

Grant MR, Godiard L, Straube E, Ashfield T, Lewald J, Sattler A, Innes RW, Dangl JL. 1995. Structure of the Arabidopsis *RPM1* gene enabling dual specificity disease resistance. *Science* **269,** 843–846.

Guan KL, Dixon JE. 1991. Eukaryotic proteins expressed in *Escherichia coli*: an improved thrombin cleavage and purification procedure of fusion proteins with glutathione S-transferase. *Analytical Biochemistry* **192,** 262–267.

Hellens R, Mullineaux P, Klee H. 2000. Technical focus: a guide to *Agrobacterium* binary Ti vectors. *Trends in Plant Science* **5,** 446–451.

Hemsley A, Arnheim N, Toney MD, Cortopassi G, Galas DJ. 1989. A simple method for site-directed mutagenesis using the polymerase chain reaction. *Nucleic Acids Research* **17,** 6545–6551.

Higuchi R, Krummel B, Saiki RK. 1988. A general method of *in vitro* preparation and specific mutagenesis of DNA fragments: study of protein and DNA interactions. *Nucleic Acids Research* **16,** 7351–7367.

Howles P, Lawrence G, Finnegan J, McFadden H, Ayliffe M, Dodds P, Ellis J. 2005. Autoactive alleles of the flax *L6* rust resistance gene induce non-race-specific rust resistance associated with the hypersensitive response. *Molecular Plant–Microbe Interactions* **18,** 570–582.

Jones JDG, Dangl JL. 2006. The plant immune system. *Nature* **444,** 323–329.

Ke SH, Madison EL. 1997. Rapid and efficient site-directed mutagenesis by single-tube 'megaprimer' PCR method. *Nucleic Acids Research* **25,** 3371–3372.

Koncz C, Schell J. 1986. The promoter of Tl-DNA gene *5* controls the tissue-specific expression of chimaeric genes carried by a novel type of *Agrobacterium* binary vector. *Molecular and General Genetics* **204,** 383–396.

Leipe DD, Koonin EV, Aravind L. 2004. STAND, a class of P-loop NTPases including animal and plant regulators of programmed cell death: multiple, complex domain architectures, unusual phyletic patterns, and evolution by horizontal gene transfer. *Journal of Molecular Biology* **343,** 1–28.

Martin GB, Bogdanove AJ, Sessa G. 2003. Understanding the functions of plant disease resistance proteins. *Annual Review of Plant Biology* **54,** 23–61.

Meyers BC, Chin DB, Shen KA, Sivaramakrishnan S, Lavelle DO, Zhang Z, Michelmore RW. 1998. The major resistance gene cluster in lettuce is highly duplicated and spans several megabases. *The Plant Cell* **10,** 1817–1832.

Meyers BC, Dickerman AW, Michelmore RW, Sivaramakrishnan S, Sobral BW, Young ND. 1999. Plant disease resistance genes encode members of an ancient and diverse protein family within the nucleotide-binding superfamily. *The Plant Journal* **20,** 317–332.

Moffett P, Farnham G, Peart J, Baulcombe DC. 2002. Interaction between domains of a plant NBS-LRR protein in disease resistance-related cell death. *EMBO Journal* **21,** 4511–4519.

Ogura T, Whiteheart SW, Wilkinson AJ. 2004. Conserved arginine residues implicated in ATP hydrolysis, nucleotide-sensing, and inter-subunit interactions in AAA and AAA+ ATPases. *Journal of Structural Biology* **146,** 106–112.

Ogura T, Wilkinson AJ. 2001. AAA+ superfamily ATPases: common structure–diverse function. *Genes Cells* **6,** 575–597.

Pan Q, Liu YS, Budai Hadrian O, Sela M, Carmel Goren L, Zamir D, Fluhr R. 2000. Comparative genetics of nucleotide binding site-leucine rich repeat resistance gene homologues in the genomes of two dicotyledons: tomato and *Arabidopsis*. *Genetics* **155,** 309–322.

Peart JR, Mestre P, Lu R, Malcuit I, Baulcombe DC. 2005. NRG1, a CC-NB-LRR protein, together with N, a TIR-NB-LRR protein, mediates resistance against Tobacco Mosaic Virus. *Current Biology* **15,** 968–973.

Rairdan GJ, Moffett P. 2006. Distinct domains in the ARC region of the potato resistance protein Rx mediate LRR binding and inhibition of activation. *The Plant Cell* **18,** 2082–2093.

Rairdan G, Moffett P. 2007. Brothers in arms? Common and contrasting themes in pathogen perception by plant NB-LRR and animal NACHT-LRR proteins. *Microbes and Infection* **9,** 677–686.

Riedl SJ, Li W, Chao Y, Schwarzenbacher R, Shi Y. 2005. Structure of the apoptotic protease-activating factor 1 bound to ADP. *Nature* **434,** 926–933.

Rohila JS, Chen M, Cerny R, Fromm ME. 2004. Improved tandem affinity purification tag and methods for isolation of protein heterocomplexes from plants. *The Plant Journal* **38,** 172–181.

Salmeron JM, Oldroyd GED, Rommens CMT, Scofield SR, Kim HS, Lavelle DT, Dahlbeck D, Staskawicz BJ. 1996. Tomato *Prf* is a member of the leucine-rich repeat class of plant disease resistance genes and lies embedded within the *Pto* kinase gene cluster. *Cell* **86,** 123–133.

Takken FLW, Albrecht M, Tameling WIL. 2006. Resistance proteins: molecular switches of plant defence. *Current Opinion in Plant Biology* **9,** 383–390.

Takken FLW, Luderer R, Gabriëls SHEJ, Westerink N, Lu R, de Wit PJGM, Joosten MHAJ. 2000. A functional cloning strategy, based on a binary PVX-expression vector, to isolate HR-inducing cDNAs of plant pathogens. *The Plant Journal* **24,** 275–283.

Tameling WIL, Elzinga SD, Darmin PS, Vossen JH, Takken FLW, Haring MA, Cornelissen BJC. 2002. The tomato *R* gene products I-2 and Mi-1 are functional ATP binding proteins with ATPase activity. *The Plant Cell* **14,** 2929–2939.

Tameling WIL, Vossen JH, Albrecht M, Lengauer T, Berden JA, Haring MA, Cornelissen BJC, Takken FLW. 2006. Mutations in the NB-ARC domain of I-2 that impair ATP hydrolysis cause autoactivation. *Plant Physiology* **140,** 1233–1245.

Tao Y, Yuan F, Leister RT, Ausubel FM, Katagiri F. 2000. Mutational analysis of the Arabidopsis nucleotide binding site-leucine-rich repeat resistance gene *RPS2*. *The Plant Cell* **12,** 2541–2554.

Ting JP, Kastner DL, Hoffman HM. 2006. CATERPILLERs, pyrin and hereditary immunological disorders. *Nature Reviews Immunology* **6,** 183–195.

Tornero P, Chao RA, Luthin WN, Goff SA, Dangl JL. 2002. Large-scale structure-function analysis of the *Arabidopsis* RPM1 disease resistance protein. *The Plant Cell* **14,** 435–450.

van der Biezen EA, Jones JDG. 1998. The NB-ARC domain: a novel signalling motif shared by plant resistance gene products and regulators of cell death in animals. *Current Biology* **8,** R226–R228.

van der Vossen E, Sikkema A, Hekkert BL, Gros J, Stevens P, Muskens M, Wouters D, Pereira A, Stiekema W, Allefs S. 2003. An ancient R gene from the wild potato species *Solanum bulbocastanum* confers broad-spectrum resistance to *Phytophthora infestans* in cultivated potato and tomato. *The Plant Journal* **36,** 867–882.

van Ooijen G, van den Burg HA, Cornelissen BJC, Takken FLW. 2007. Structure and function of resistance proteins in solanaceous plants. *Annual Review of Phytopathology* **45,** 43–72.

Vriend G. 1990. WHAT IF: a molecular modeling and drug design program. *Journal of Molecular Graphics* **8,** 52–56.

Yan N, Chai J, Lee ES, *et al*. 2005. Structure of the CED-4-CED-9 complex provides insights into programmed cell death in *Caenorhabditis elegans*. *Nature* **437,** 831–837.

Ye Y, Godzik A. 2003. Flexible structure alignment by chaining aligned fragment pairs allowing twists. *Bioinformatics* **19,** Supplement 2, II246–II255.